Comparison of magnetic phase diagrams for $(Mn_{1-x}Fe_x)Pt_3$ alloys in the ordered and disordered states

1994 J. Phys.: Condens. Matter 6 791

(http://iopscience.iop.org/0953-8984/6/3/019)

J. Phys.: Condens. Matter 6 (1994) 791–800. Printed in the UK

Comparison of magnetic phase diagrams for $(Mn_{1-x}Fe_x)Pt_3$ alloys in the ordered and disordered states

A Z Menshikov and G P Gasnikova

Institute of Metal Physics, Urals Branch of the Russian Academy of Sciences, 620219, GSP-170, S Kovalevskoi Street 18, Ekaterinburg, Russia

Received 21 June 1993, in final form 1 September 1993

Abstract. Magnetic phase transitions as a function of concentration and temperature for ordered and disordered $(Mn_{1-x}Fe_x)Pt_3$ alloys are investigated by neutron diffraction and magnetic measurements. On the basis of these results the magnetic phase diagrams are drawn. The diagram for the ordered alloys is characterized by a tricritical point in the region of the ferromagnetic-to-antiferromagnetic transition at $X_c = \frac{2}{3}$. A canted non-collinear magnetic structure and a region of two-phase mixtures are shown. The diagram for the disordered alloys is characterized by two regions of heterogeneous ferromagnets, both showing re-entrant spin-glass states at low temperatures, but differing in the character of exchange interaction between magnetic atoms. The diagrams are discussed within the framework of the phenomenological theory of the phase transitions with related order parameters.

1. Introduction

In early papers [1,2] it was shown that ordered alloys of iron and manganese with such noble metals as palladium and platinum are unique magnetic systems, in which a concentration phase transition from ferromagnetism to antiferromagnetism is realized within the framework of a continuous series of solid solutions. Because of this they are convenient experimental objects for verifying theoretical models of magnetic phase transitions in systems with related magnetic order parameters [3,4].

Ordered and disordered $(Mn_{1-x}Fe_x)Pt_3$ alloys are typical of the above systems and their magnetic state has been investigated in [5–12]. The components form a continuous series of solid solutions and can be transformed from a system with random magnetic sites and a simple-cubic structure to a FCC lattice through an order–disorder transition provided that the magnetic moment of the platinum atom equals zero. Therefore, we have a possibility of comparing the magnetic phase diagrams for random magnetic systems with one sort of magnetic atom and which have different crystal symmetry lattices. This dependence on symmetry is caused by the probability of formation of frustrated sites, which in the case of a FCC lattice is greater than for systems with a simple-cubic lattice [13].

The purpose of the present work is to study in more detail the magnetic states of $(Mn_{1-x}Fe_x)Pt_3$ alloys in the region of the concentration-dependent transition from ferromagnetic to antiferromagnetic order and to compare the magnetic phase diagrams for the ordered and disordered states.

0953-8984/94/030791+10$07.50

2. Methods

Quasi-binary alloys of $(Mn_{1-x}Fe_x)Pt_3$ with $x = 0$, 0.15, 0.2, 0.3, 0.4, 0.45, 0.55, 0.6, 0.65, 0.7, 0.75, 0.8 or 1.0 were melted from pure components. The ingots were homogenized at 1250 K for 5 d in a helium atmosphere. They were then crushed into powder, in which form the alloys are completely disordered. The atomic ordered state was obtained after annealing of the deformed samples at 920 K for 48 h in a helium atmosphere.

The degree of atomic ordering was determined from the x-ray and elastic neutron scattering data at room temperature and 4.2 K respectively. The degree of ordering calculated from these data turned out to be nearly complete. It should be noted that the ordering of samples which were not deformed initially, as a rule, gave a smaller degree of ordering.

Information about the magnetic state of the alloys was obtained by magnetic neutron scattering ($\lambda = 0.181$ nm) and bulk magnetic measurements. The latter were made with a vibromagnetometer in fields of $(0.008–1.6) \times 10^6$ A m^{-1} within the temperature range 4.2–300 K. The differential magnetic AC susceptibility was measured with a modified Harsthorn bridge at 5 Gz in a zero magnetic field within the temperature range 20–200 K.

3. Results

3.1. Magnetic phase diagram for the ordered $(Mn_{1-x}Fe_x)Pt_3$ alloys

According to the x-ray study, all the alloys after annealing have $L1_2$-type atomic order with an ordering degree in the platinum sublattice of 0.96–0.98. Moreover, the large difference between the nuclear scattering amplitudes of iron and manganese allows us to show that iron and manganese atoms are distributed randomly in a simple-cubic lattice.

The antiferromagnetic long-range order with the wavevector $k = (2\pi/a)(\frac{1}{2}, \frac{1}{2}, 0)$ was determined by elastic neutron scattering for alloys with $x \geqslant 0.55$. The region of this antiferromagnetic order is determined from the temperature dependence of the $(\frac{1}{2}, \frac{1}{2}, 0)$ reflection (figure 1). Moreover, additional magnetic contributions to the superstructure in the form of (100) nuclear reflections testify to the long-range ferromagnetic order for the alloys with $x \leqslant 0.45$. Figure 1 shows that these ferromagnetic contributions to the superstructure are also present in alloys in the transition region from ferromagnetism to antiferromagnetism ($0.55 < x \leqslant 0.65$) near the respective Néel temperatures. The spin moment values $\bar{\mu}$ at the averaged (Fe, Mn) atom sites, determined from the intensity of the corresponding ferromagnetic and antiferromagnetic reflections, are determined from the relation $\bar{\mu}^2 = \mu_F^2 + \mu_{AF}^2$ at 4.2 K. They are well fitted by the mixing law $\bar{\mu} = \mu_{Mn}(1 - x) + \mu_{Fe}x$ with $\mu_{Mn} = 4.2\ \mu_B$ and $\mu_{Fe} = 3.3\ \mu_B$.

The iron concentration region $x = 0.45–0.7$ is interesting because of contradictory results in different papers. Detailed investigations of the temperature dependence of DC susceptibility for the alloys cooled to 4.2 K in zero (χ_{ZFC}) and measuring (χ_{FC}) magnetic fields were made. Figure 2 shows that pronounced differences between the $\chi_{ZFC}(T)$ and $\chi_{FC}(T)$ curves occur between certain temperatures $T_B(H)$ for all the alloys within the critical range. The appearance of magnetic irreversibility indicates the presence of non-ergodic states in the magnetic system below $T_B(H)$. Moreover, the Sommers–Sompolinsky non-ergodicity parameter $\bar{\Delta} = \chi_{ZFC}(0) - \chi_{FC}(0)$ changes sharply at some critical concentration $x_c = \frac{2}{3}$, showing a ferromagnetic-to-antiferromagnetic first-order phase transition (figure 3). The critical concentration $x_c = \frac{2}{3}$ is caused by the presence of a ferromagnetic interaction between Mn–Mn and Mn–Fe atoms and antiferromagnetic interaction in Fe–Fe pairs in a

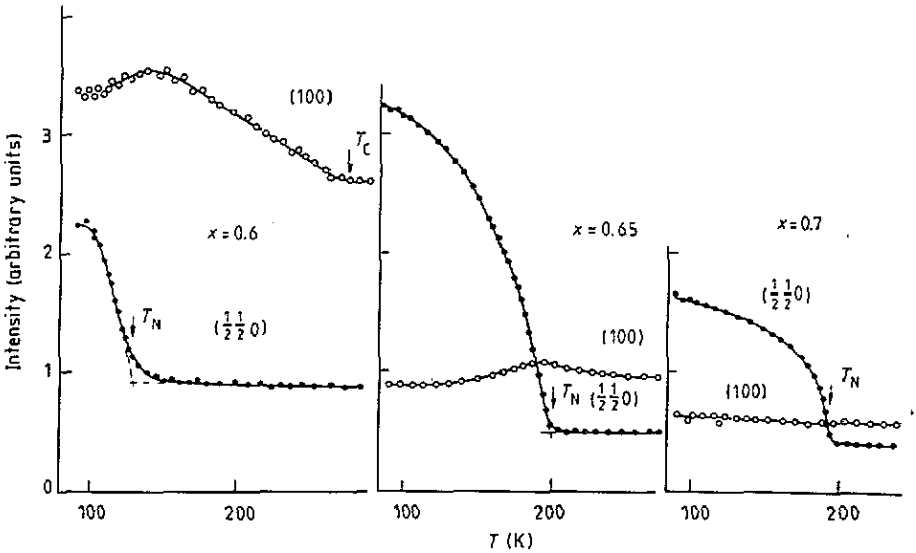

Figure 1. Temperature dependence of the neutron scattering intensity of ferromagnetic (100) and antiferromagnetic $(\frac{1}{2}\frac{1}{2}0)$ reflections for ordered $(Mn_{1-x}Fe_x)Pt_3$ alloys.

simple-cubic lattice, which is equivalent to an interaction between nearest neighbours in a FCC lattice ($J^{NNN}_{Mn-Mn} > 0$, $J^{NNN}_{Mn-Fe} > 0$ and $J^{NNN}_{Fe-Fe} < 0$), the presence of $\frac{2}{3}$ ferromagnetic bonds from the six possible ($z = 6$) leads to a sharp ferromagnetic-to-antiferromagnetic transition at the iron concentration $x_c = \frac{2}{3}$. In other words, at a critical concentration x_c the contributions of the positive exchange interaction and the negative exchange interaction to the crystal free energy are equal. This leads to the relation

$$x_c^2 J_{Fe-Fe} S_{Fe}^2 = (1 - x_c)^2 J_{Mn-Mn} S_{Mn}^2 + 2x_c(1 - x_c) J_{Fe-Mn} S_{Fe} S_{Mn}.$$

Substituting the numerical values of x_c S_{Mn} and S_{Fe} and also assuming that $J_{Mn-Mn} \simeq J_{Fe-Mn}$, we obtain $|J_{Fe-Fe}| \simeq 2J_{Mn-Mn}$.

The magnetic ground state of alloys near the critical concentration is more complicated than the ferromagnetic or antiferromagnetic state. As we noted already, for alloys in the region $0.45 \leqslant x \leqslant 0.65$ antiferromagnetic ordering is found at temperatures $T < T_m$. Their state may be characterized as a canted magnetic structure with a translational invariance of both the ferromagnetic and the antiferromagnetic components of the magnetic structure, described by the wavevectors $k_F = (2\pi/a)(0, 0, 0)$ and $k_{AF} = (2\pi/a)(\frac{1}{2}, \frac{1}{2}, 0)$.

It is necessary to note that in [7, 8] the magnetic state of these alloys was identified with a re-entrant spin-glass state, in which ferromagnetic blocks about 500–1000 Å in size are formed. However, the presence of the antiferromagnetic reflection $(\frac{1}{2}\frac{1}{2}0)$ in our neutron results proves unambiguously that within the boundaries of such a block, essentially exceeding the range of coherent neutron scattering (about 200 Å), antiferromagnetic long-range order exists. Consequently, the magnetic state of these alloys with regard to these blocks must be described by two order parameters, ferromagnetic and antiferromagnetic, simultaneously.

Such a canted magnetic structure of the alloy may be like a re-entrant spin-glass phase, since after cooling in a magnetic field a unidirectional anisotropy forms because of the non-collinearity of the magnetic structure, which can be seen from a displacement of the

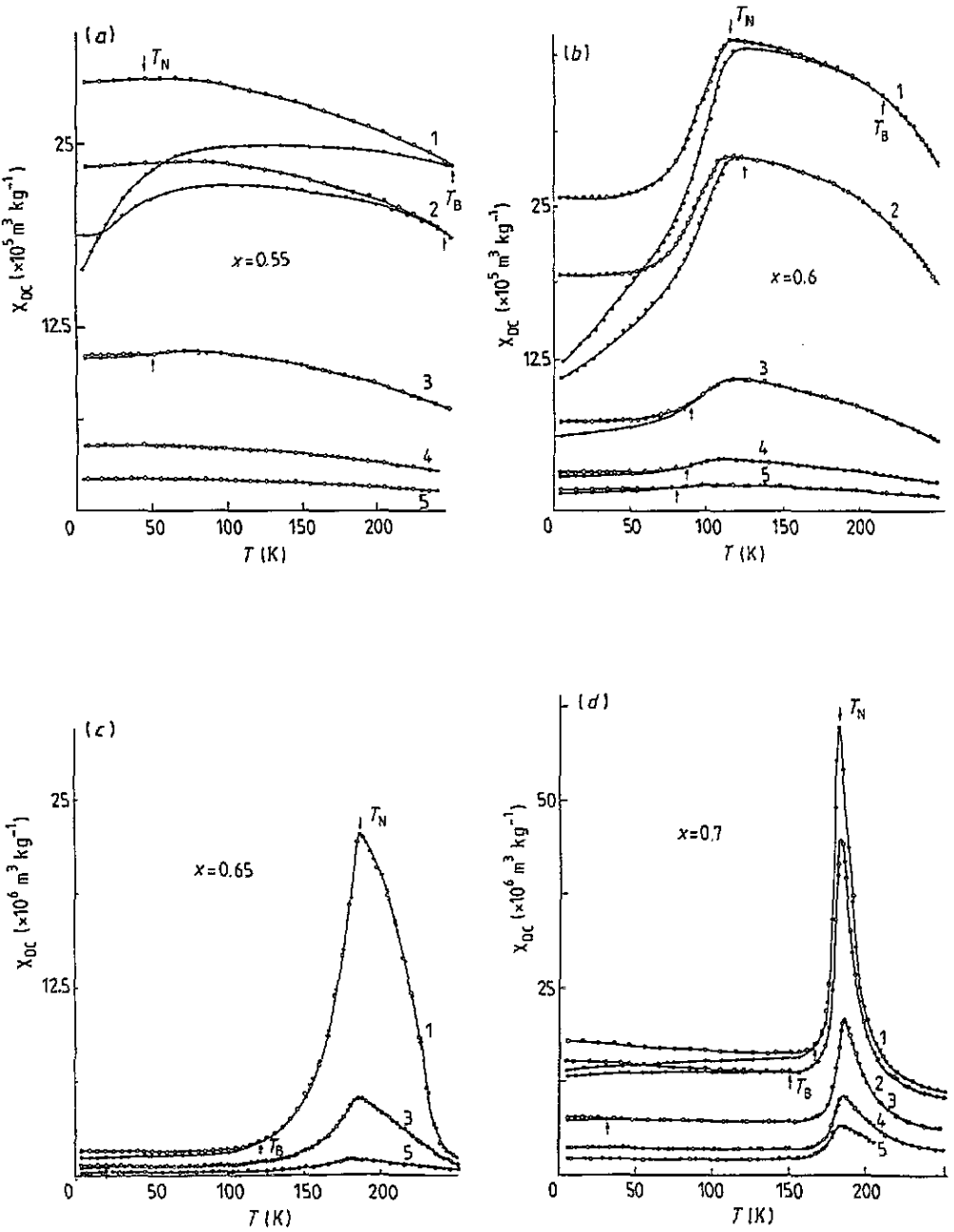

Figure 2. Temperature dependence of the DC susceptibility, obtained for ordered $(Mn_{1-x}Fe_x)Pt_3$ alloys with x-values of (*a*) 0.55, (*b*) 0.6, (*c*) 0.65, (*d*) 0.7 and (*e*) 0.75 after cooling to 4.2 K in zero (●) and measuring (○) magnetic fields: curves 1, H = 0.04 A m^{-1}; curves 2, H = 0.08 A m^{-1}; curves 3, H = 0.28 A m^{-1}; curves 4, H = 0.72 A m^{-1}; curves 5, $H = 1.6 \times 10^6$ A m^{-1}.

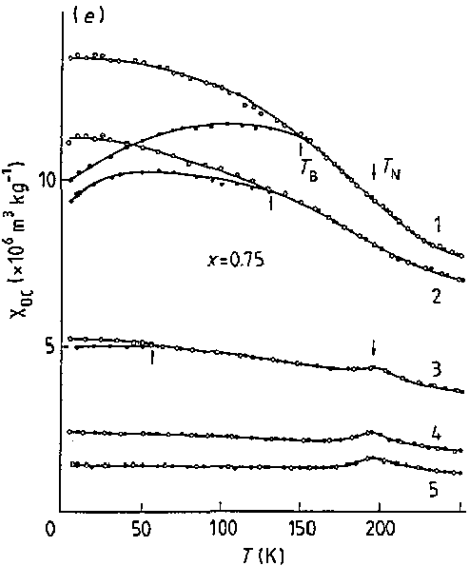

Figure 2. (Continued)

magnetic hysteresis loop and magnetic viscosity effects. The neutron data unambiguously prove the presence of a canted structure, but the measurements of magnetic and thermal properties are less certain indicators.

In a composition region above the critical concentration $x_c = \frac{2}{3}$ we have observed the presence of heterogeneous antiferromagnetism, characterized by ferromagnetic clusters in the antiferromagnetic matrix. This agrees with the results of [7, 8]. It follows from the large magnetic susceptibility for the alloys with $0.65 < x < 0.8$ at low temperatures and a susceptibility irreversibility at $T < T_N$.

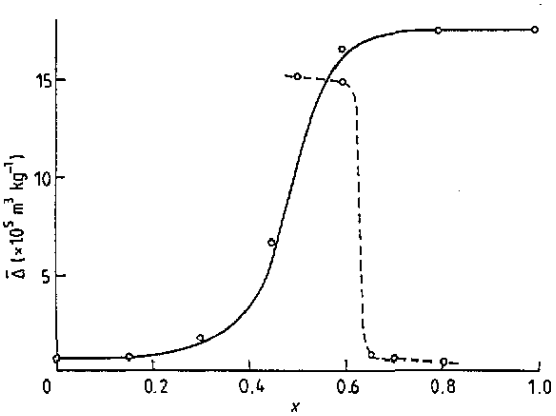

Figure 3. Concentration dependence of the Sommers–Sompolinsky parameter $\bar{\Delta}$ for ordered (----) and disordered (——) $(Mn_{1-x}Fe_x)Pt_3$ alloys for $H = 0.04 \times 10^6$ A m^{-1} at 4.2 K.

From the present elastic neutron scattering and magnetic measurement data, together with data from other investigations, the magnetic phase diagram for the ordered

$(Mn_{1-x}Fe_x)Pt_3$ alloys has been drawn (figure 4). The main feature of this diagram is the tricritical point with the coordinates $x_c = 0.65$ and $T = 260$ K, where the line of the second-order phase transition transforms into two lines of the first-order phase transitions.

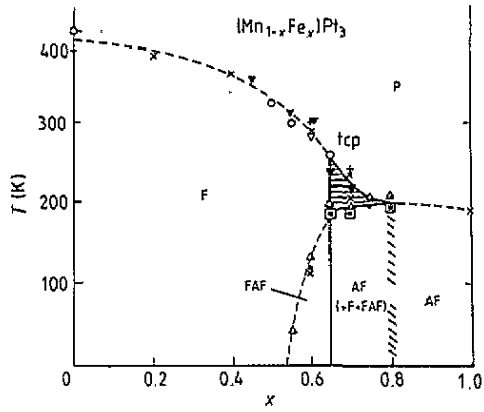

Figure 4. Magnetic phase diagram for ordered $(Mn_{1-x}Fe_x)Pt_3$ alloys: P, paramagnetic phase; F, ferromagnetic phase; AF, antiferromagnetic phase; FAF, canted magnetic structure; AF(+F + FAF), mixture of magnetic phases; tcp, tricritical point; shaded area, F + P mixture.

In the region below the critical concentration $x_c = \frac{2}{3}$, a phase F with a ferromagnetic order parameter and a mixed phase FAF described by two order parameters simultaneously, are indicated. For the alloys with $x > x_c$, the region of the high-temperature mixture F + P of ferromagnetism and paramagnetism (shaded regions in figure 4) is also shown. The paramagnetic phase of this mixed state transfers into an antiferromagnetic phase below some temperature T_N, increasing with increasing x. The ferromagnetic phase decreases to dimensions smaller than the coherent neutron scattering ranges (about 100–200 Å), since the additional scattering intensity is absent in the superstructure reflections for the alloys with $x \geqslant 0.8$. The magnetic state in the region $0.66 \leqslant x \leqslant 0.8$ is labelled AF(+F + FAF).

3.2. Magnetic phase diagram for the disordered $(Mn_{1-x}Fe_x)Pt_3$ alloys

According to the x-ray and neutron scattering data the alloys really have the FCC lattice structure without any signs of atomic ordering following mechanical crushing. Weak neutron diffraction peaks are obtained in the positions of superstructure reflections (100) and (110) only for the alloys with $x = 0.0$ and 0.15. These arise from traces of $MnPt_3$-type atomic ordering.

Detailed investigation of elastic neutron scattering indicates an absence of any long-range antiferromagnetic order in these alloys. Therefore the main conclusions concerning the magnetic state of the disordered alloys are drawn from the magnetic measurements.

Figure 5. (Opposite.) Temperature dependence of DC susceptibility, obtained for disordered $(Mn_{1-x}Fe_x)Pt_3$ alloys with x-values of (*a*) 0.15, (*b*) 0.45, (*c*) 0.6 and (*d*) 0.8 after cooling in zero (●) and measuring (○) magnetic fields: curves 1, $H = 0.04$ A m^{-1}; curves 2, $H = 0.08$ A m^{-1}; curves 3, $H = 0.28$ A m^{-1}; curves 4, $H = 0.72$ A m^{-1}; curves 5, $H = 1.6 \times 10^6$ A m^{-1}; ↑, $T_B(H)$; ↓, $T_f(H)$.

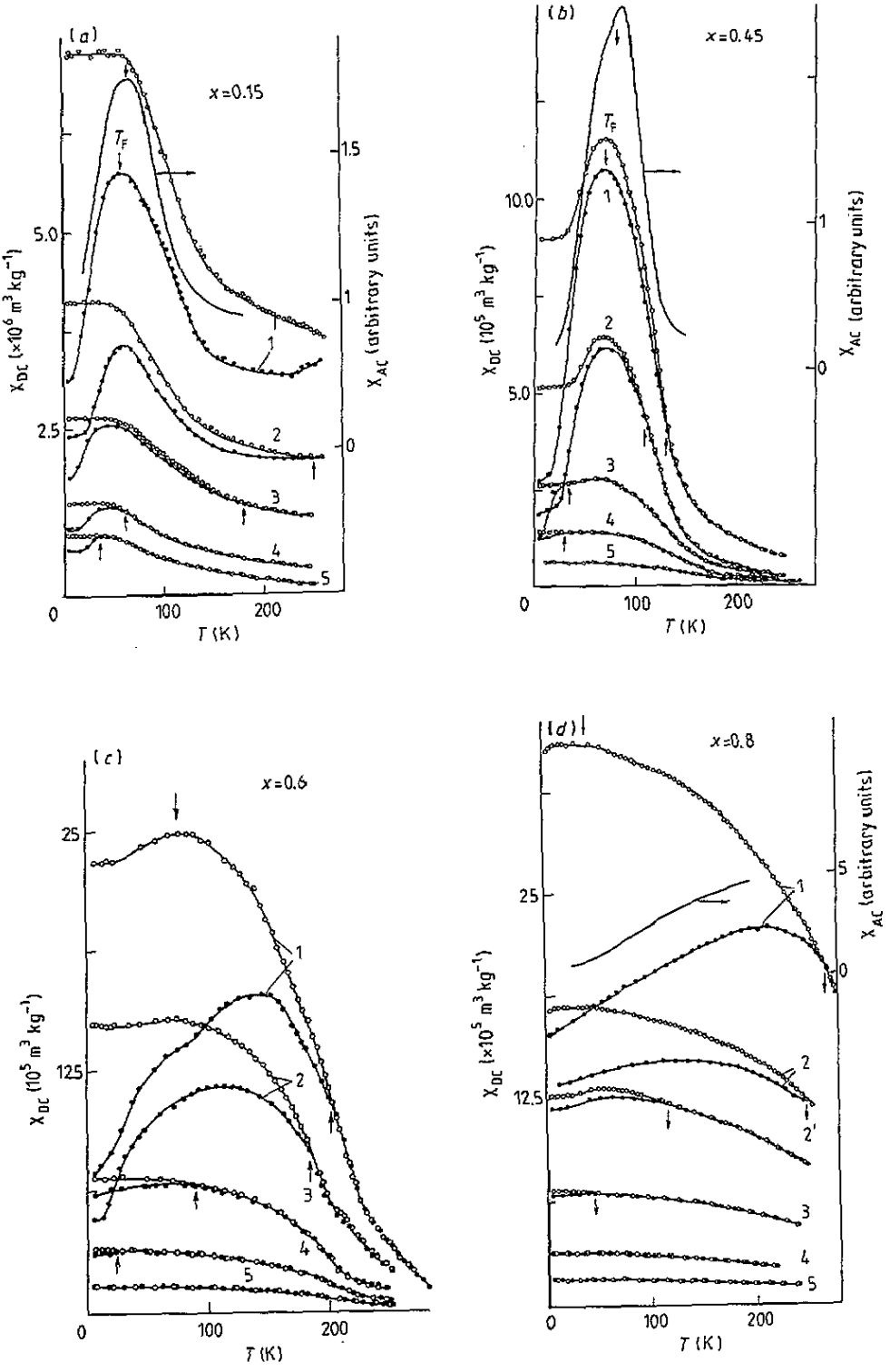
(a)
x=0.15
T_F
1
2
3
4
5
5.0
2.5
1.5
1
0
0
100
200
T (K)
χ_{DC} ($\times 10^6$ m^3 kg^{-1})
χ_{AC} (arbitrary units)
(b)
x=0.45
10.0
5.0
χ_{DC} (10^5 m^3 kg^{-1})
(c)
x=0.6
25
12.5
(d)
x=0.8
2'

The alloys with $x < 0.5$ have a weak magnetization at 4.2 K, which increases with increasing x above $x = 0.5$. The essential difference between the temperature dependences $\chi_{ZFC}(T)$ and $\chi_{FC}(T)$ indicates the presence of heterogeneous ferromagnetism (figure 5) in these alloys. The magnetic irreversibility for the alloys with $x > 0.5$ is slightly different. They have a large spontaneous magnetization, and the $\bar{\Delta}$-values are essentially larger than those of the alloys with $x < 0.5$ (figure 3). This points to the existence of a critical concentration $x_c = 0.5$ for the magnetic state with spontaneous magnetization for the disordered alloys.

However, the alloys with $x > 0.5$ are not homogeneous ferromagnets, because the temperature T_k of the transition from the paramagnetic to the ferromagnetic state (obtained from magnetization curves by the Belov–Arrot method), and the temperature $T_B(0)$ at which irreversibility occurs (determined by the $T_B(H)$ extrapolation to zero field) coincide. Such a state may be represented as the sum of a topologically infinite ferromagnetic cluster and some finite ferromagnetic clusters. Between them there exists a zone of slowly relaxing spins, disposed in a zero molecular magnetic field ('melted spins' [14]). In the magnetic phase diagram (figure 6) this state is labelled F(+P). With decreasing temperature, the relaxation time of the 'melted' spins increases but at the temperature $T_F(0)$ corresponding to the occurrence of 'strong' irreversibility, critical slowing-down of the weakly relaxing spins occurs because of an antiferromagnetic interaction at low temperatures. This is accompanied by the occurrence of the local magnetization $\langle S_i \rangle_T = m_i$ for the 'melted' spins. This magnetization may be considered as a random magnetic field H_a for the topologically infinite ferromagnetic cluster. When the random field H_a becomes comparable with the anisotropy field H_k of the topologically infinite cluster, the latter falls into clusters of finite sizes L with a random magnetization distribution in space. This re-entrant ferromagnetic spin-glass state FSG″ may be described by a parameter $Q^F = \langle \mu_j^2 \rangle_c$, $\langle \mu_j \rangle_c = 0$ where μ_j is the magnetic moment of a finite cluster. Here $\langle \ldots \rangle_T$ and $\langle \ldots \rangle_c$ are the temperature and configurational averages, respectively.

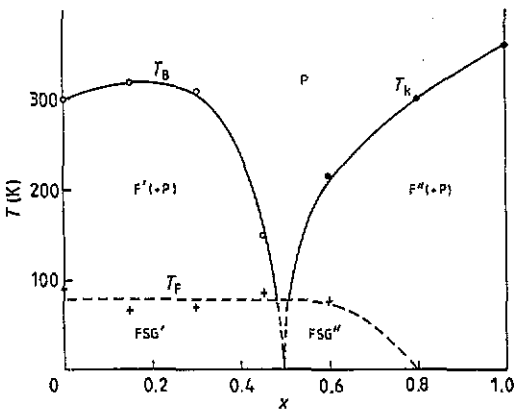

Figure 6. Magnetic phase diagram for disordered $(Mn_{1-x}Fe_x)Pt_3$ alloys: F′(+P) and F″(+P), heterogeneous ferromagnetic phases; FSG′ and FSG″, re-entrant spin-glass states.

In the concentration region $x < x_c$ the magnetic state does not show a spontaneous magnetization. This is consistent with small ferromagnetic clusters with magnetic moments chaotically reoriented inside a system with slowly relaxing spins close to a paramagnetic

state. This system labelled P(+F') shows magnetization irreversibility, which is 'weak' at temperatures near $T_k = T_B(0)$, and 'strong' at $T_F(0)$. The phase transition takes place at $T_B(0)$ in the ferromagnetic clusters system, but at $T_F(0)$ the critical slowing of the relaxation time for 'melted' spins occurs. This leads to a splitting of the large ferromagnetic clusters into smaller clusters, and their blocking in the random anisotropy field. This state labelled FSG' is a ferromagnetic spin glass.

However, the natures of FSG' and FSG'' (and also F' and F'') differ because of the different exchange interactions between magnetic atoms. In the first case, the finite-cluster ferromagnetism is caused by the $MnPt_3$-type short-range order and the ferromagnetic interaction between manganese atoms of next-nearest-neighbour distance ($J_{Mn-Pt-Mn} > 0$). In the second case, the ferromagnetism is caused by a strong positive exchange interaction between iron atoms of nearest-neighbour distance ($J_{Fe-Fe} > 0$).

4. Discussion

Let us consider now the magnetic phase diagram for the ordered and disordered $(Mn_{1-x}Fe_x)Pt_3$ alloys constructed here, from the point of view of the phenomenological theory of the phase transitions in systems with related order parameters [3, 4]. First, we discuss the magnetic phase diagram for the ordered $(Mn_{1-x}Fe_x)Pt_3$ alloys. We choose the ferromagnetism vectors $\boldsymbol{m} = \boldsymbol{M}_1 + \boldsymbol{M}_2$ and antiferromagnetism vectors $\boldsymbol{l} = \boldsymbol{M}_1 - \boldsymbol{M}_2$, where $\boldsymbol{M}_1$ and $\boldsymbol{M}_2$ are the magnetizations of two sublattices, as the vector order parameters. The distortion of the cubic lattice because of magnetoelastic interaction is chosen as the scalar order parameter u_{ik}.

The thermodynamic potential of a system with two related vector order parameters and one scalar order parameter is

$$\Phi = \Phi_0 + 1/2A_1|\boldsymbol{m}_1|^2 + 1/4C_1|\boldsymbol{m}|^4 + 1/6E|\boldsymbol{m}|^6 + 1/2A_2|\boldsymbol{l}|^2 + 1/4C_2|\boldsymbol{l}|^4 + 1/2A_3u_{ik}^2 + \lambda^2|\boldsymbol{m}|^2|\boldsymbol{l}|^2 + \gamma|\boldsymbol{m}|^2u_{ik} \quad (1)$$

where λ is the constant of the relation between vector order parameters and γ is the constant of the magnetoelastic interaction in the ferromagnetic subsystem. A consideration of such a potential leads to the following equilibrium phases in the diagram:

(1) paramagnetic phase ($\boldsymbol{m} = \boldsymbol{0}$; $\boldsymbol{l} = \boldsymbol{0}$);
(2) ferromagnetic phase ($\boldsymbol{m} \neq \boldsymbol{0}$; $\boldsymbol{l} = \boldsymbol{0}$);
(3) antiferromagnetic phase ($\boldsymbol{m} = \boldsymbol{0}$; $\boldsymbol{l} \neq \boldsymbol{0}$);
(4) mixed phase ($\boldsymbol{m} \neq \boldsymbol{0}$; $\boldsymbol{l} \neq \boldsymbol{0}$) and also phase mixtures F + P and F + AF + FAF.

The phase diagrams, constructed for different values of the parameters λ, $C = C_1 - 2\gamma^2/A_3$ and $\Delta = C_1C_2 - \lambda^2$ and their branches in temperature–composition coordinates were given in [3, 4]. The phase diagram for the ordered $(Fe_{1-x}Mn_x)Pt_3$ alloys corresponds most closely to the case $\lambda < 0$, $C_1 < 0$ and $\Delta < 0$. This is characteristic for systems with a strong relation between the vector order parameters and the scalar order parameter.

As to the phase diagram for the $(Mn_{1-x}Fe_x)Pt_3$ alloys in a disordered state, we propose the existence of two independent ferromagnetic order parameters. One of them, namely $\boldsymbol{m}'$ describes the alloys with a large manganese content, where the exchange interactions $J_{Mn-Pt-Mn} > 0$, $J_{Mn-Pt-Fe} > 0$ and $J_{Fe-Pt-Fe} < 0$ are essential. The other order parameter $\boldsymbol{m}''$ describes the alloys with a large iron content in which the exchange interactions $J_{Fe-Fe} > 0$, $J_{Fe-Mn} > 0$ and $J_{Mn-Mn} < 0$ between nearest neighbours play a general

role. The magnetic phase diagram for such alloys must be attributed to the case of the non-interacting vector order parameters ($\lambda = 0$). Then the thermodynamic potential (1) can be separated into two independent potentials, where the interaction of each vector order parameter with its own scalar appears in general. Such a situation, as a rule, leads to the formation of composition ranges with a tricritical behaviour, where the transition to a re-entrant spin-glass state takes place.

5. Conclusion

Magnetic phase diagrams for the ordered and disordered $(Mn_{1-x}Fe_x)Pt_3$ alloys considered here differ markedly. This mainly originates from the different crystallographic symmetries for the magnetic iron and manganese atoms. The probability of formation of frustrated sites for the ordered alloys with a simple-cubic symmetry of magnetic atoms is smaller than in disordered alloys [15]. This leads to the strong interaction of the vector order parameters in the systems with a simple-cubic lattice, while in systems with a FCC symmetry this interaction is small or equals zero. As a result, in the phase diagram for such systems, the spin-glass state is present in the range of a transition from one magnetic order to the other.

Acknowledgments

The authors express their gratitude to professor E F Wassermann for useful discussion and his comments on the manuscript. The work was carried out with support from the Russian Fundamental Research Fund (93-02-2808).

References

[1] Kouvel J S and Forsyth J B 1969 *J. Appl. Phys.* **40** 1359
[2] Bacon G E and Mason E M 1966 *Proc. Phys. Soc.* **88** 929
[3] Gufan Yu M and Larin E F 1980 *Fiz. Tverd. Tela.* **22** 463
[4] Menshikov A Z 1988 *Physica* B **149** 249
[5] Vokhmyanin A P, Kelarev V V, Pirogov A N and Sidorov S K 1978 *Fiz. Metall. Metalloved.* **46** 67
[6] Vokhmyanin A P, Kelarev V V, Pirogov A N, Chuev V V and Sidorov S K 1980 *Fiz. Metall. Metalloved.* **50** 1010
[7] Schreiner W H, Stamm W and Wassermann E F 1985 *J. Phys. F: Met. Phys.* **15** 2009
[8] Stamm W and Wassermann E F 1986 *J. Magn. Magn. Mater.* **54–57** 161
[9] Gasnikova G P and Menshikov A Z 1990 *Fiz. Metall. Metalloved.* **11** 103
[10] Gasnikova G P and Menshikov A Z 1992 *Fiz. Metall. Metalloved.* **9** 64
[11] Kourov N I, Tsiovkin Yu N and Volkenshtein N V 1983 *Fiz. Metall. Metalloved.* **55** 955
[12] Podgornych S M, Kourov N I, Tsiovkin Yu N and Volkenshtein N V 1984 *Fiz. Metall. Metalloved.* **58** 265
[13] Medvedev M V and Zaborov A V 1981 *Fiz. Metall. Metalloved.* **52** 272, 472, 942
[14] Saslov W M and Parker G 1986 *Phys. Rev. Lett.* **56** 1074
[15] Medvedev M V and Sadovsky M V 1982 *Phys. Status Solidi* b **109** 49